



Providing Choice & Value

Generic CT and MRI Contrast Agents



**FRESENIUS
KABI**

CONTACT REP

AJNR

**Revisiting the Pathophysiology of
Intracranial Hemorrhage in Fetuses with
Chiari II Malformation: Novel Imaging
Biomarkers of Disease Severity?**

Hui Shi, Daniela Prayer, Patric Kienast, Farjad Khalaveh,
Johannes Tischer, Julia Binder, Michael Weber, Marlene
Stuempflen and Gregor Kasprian









This information is current as
of July 30, 2025.

AJNR Am J Neuroradiol 2024, 45 (10) 1562-1569

doi: <https://doi.org/10.3174/ajnr.A8331>

<http://www.ajnr.org/content/45/10/1562>

Revisiting the Pathophysiology of Intracranial Hemorrhage in Fetuses with Chiari II Malformation: Novel Imaging Biomarkers of Disease Severity?

Hui Shi,  Daniela Prayer,  Patric Kienast,  Farjad Khalaveh,  Johannes Tischer,  Julia Binder,  Michael Weber,  Marlene Stuempflen, and  Gregor Kasprian



ABSTRACT

BACKGROUND AND PURPOSE: Intracranial hemorrhage (ICH) has emerged as a notable concern in Chiari II malformation (CM II), yet its origins and clinical implications remain elusive. This study aims to validate the in utero prevalence of ICH in CM II and investigate contributing factors, and visualize the findings in a network format.

MATERIALS AND METHODS: A single-center retrospective review of fetal MRI scans obtained in fetuses with CM II (presenting January 2007 to December 2022) was performed for ICH utilizing EPI-T2* blood-sensitive sequence. Fetuses with aqueduct stenosis (AS) were included as a control group. The incidence of ICH and corresponding gestational ages were compared between CM II and AS cases, and morphometric measurements (inner/outer CSF spaces, posterior fossa, venous structure) were compared among the 4 1:1 age-matched groups: CM II+ICH, CM II-ICH, AS+ICH, and AS-ICH. Additionally, a co-occurrence network was constructed to visualize associations between phenotypic features in ICH cases.

RESULTS: A total of 101 fetuses with CM II and 90 controls with AS at a median gestational age of 24.4 weeks and 22.8 weeks ($P = .138$) were included. Prevalence of ICH in fetuses with CM II was higher compared with the AS cases (28.7% versus 18.9%, $P = .023$), accompanied by congested veins (deep vein congestion mainly in young fetuses, and cortical veins may also be affected in older fetuses). ICH was notably correlated with specific anatomic features, essentially characterized by reduced outer CSF spaces and clivus-supraocciput angle. The co-occurrence network analysis reveals complex connections including bony defects, small posterior fossa dimensions, vermis ectopia, reduced CSF spaces, as well as venous congestion and venous sinus stenosis as pivotal components within the network.

CONCLUSIONS: The high prevalence of ICH—detected by fetal MRI—among fetuses with CM emphasizes the pathophysiologic importance of venous congestion, ICH, and vasogenic edema. As indicators of disease severity, these features may serve as helpful additional imaging biomarkers for the identification of potential candidates for fetal surgery.

ABBREVIATIONS: AS = aqueduct stenosis; CM II = Chiari type II malformation; ICH = intracranial hemorrhage; PCA = principal component analysis; SSFP = steady-state free precession; SSSFE = single-shot fast spin-echo

Chiari II malformation (CM II), a primary disorder of segmentation of the embryonic neural tube into neuromeres¹ is often associated with hydrocephalus and aqueduct stenosis (AS). In addition to the spinal defect, this malformation is associated with a complex interplay of factors in the brain, including

constriction of the posterior cranial fossa structures,² ectopic vermis, impaired venous return,³ and disturbed CSF dynamics^{3,4} during fetal stage. This intricate relationship may create a vicious cycle,⁵ perpetuating the pathophysiologic processes underlying this condition.

In previous studies, intracranial hemorrhage (ICH) has been identified as a notable concern in fetuses with CM II,^{6,7} but its etiology remains unclear. Hindbrain herniation and its close association with ventriculomegaly were presumed potential contributing factors.⁶

The presence of venous sinus stenosis³ and “lemon head” characteristics in CM II suggests shared mechanisms with craniosynostosis⁸ and Chiari I malformation.^{5,9} These parallels hint at common underlying factors affecting venous drainage. ICH could be a potential consequence of venous congestion/hypertension in

Received February 14, 2024; accepted after revision May 2.

From the Department of Radiology (H.S.), Zhu Jiang Hospital, Southern Medical University, Guangzhou, China; Departments of Biomedical Imaging and Image-guided Therapy (D.P., P.K., J.T., M.W., M.S., G.K.), Neurosurgery (F.K.), and Obstetrics and Feto-maternal Medicine (J.B.), Medical University of Vienna, Vienna, Austria.

Please address correspondence to Prof. Gregor Kasprian, MD, MBA, Department of Biomedical Imaging and Image-guided Therapy, Medical University of Vienna, Währinger Gürtel 18-20, 1090 Vienna, Austria; e-mail: gregor.kasprian@meduniwien.ac.at



Indicates article with online supplemental data.

<http://dx.doi.org/10.3174/ajnr.A8331>

SUMMARY

PREVIOUS LITERATURE: Intracranial hemorrhage is commonly detected by sonography and MR imaging in prenatal evaluation of Chiari II malformation and is frequently described on postnatal MR imaging. Prenatal ICH is associated with prenatal and postnatal hindbrain herniation likely related to its close association with increased ventriculomegaly.

KEY FINDINGS: Vermis ectopia, skull remodeling, and altered CSF dynamics may result in dural sinus stenosis, venous congestion, and intracranial hypertension, which may contribute to ICH in fetuses with CM II. Prenatal-identified ICH is correlated to more postnatal clinical morbidities and disabilities.

KNOWLEDGE ADVANCEMENT: Along with pathophysiologic alterations underlying a more severe imaging phenotype in CM II, ICH in fetuses with CM II should be considered an imaging biomarker for future neurologic morbidity in prospective fetal surgery trials.

CM II. However, specific imaging correlates between ICH and venous sinus alterations remain unexplored. A deeper understanding of these shared mechanisms could elucidate the clinical implications of ICH in CM II and influence prenatal surgical decision-making. In some institutions, ICH is even considered an exclusion criterion for surgery due to being deemed “unrelated to primary disease.”¹⁰

In exploring the potential clinical significance of ICH in fetuses with CM II, we aim to delve deeper into the underlying pathophysiology. Given the rarity of ICH occurrences in a normal cohort, we were seeking to use another condition with certain similarities to CM II to shed more light on the mechanism of ICH. By comparing the location and distinct features of ICH, CSF spaces, osseous architecture, and venous structure changes in another cohort characterized by hindered CSF circulation, we endeavor to elucidate whether obstructive hydrocephalus singularly accounts for hemorrhage, as hypothesized, or if additional factors contribute beyond the high stretch of the immature ependyma. Our study followed 3 primary objectives: validating the prevalence of brain hemorrhages in CM II through an extensive cohort analysis, exploring factors contributing to ICH based on

morphometric measurement and a comparison with AS cases, and constructing a comprehensive model elucidating contributing factors utilizing co-occurrence network analysis.

MATERIALS AND METHODS

Participants

This retrospective single-center study was approved by the institutional internal review board (Ethics Committee number 1716/2017).

Inclusion criteria for the study were the presence of CM II as characterized by the lemon configuration of the fetal head, small posterior fossa, cerebellar ectopia, kinking of the brainstem, and reduced external CSF spaces.¹ Due to the local center’s long-standing history of fetal imaging, our database of over 8000 fetal MRI examinations between January 1, 2007, and December 31, 2022, was retrospectively evaluated and cases fulfilling the criteria of a CM II malformation were included in this study. Additionally, fetuses with congenital AS (presumed hemorrhagic/infection/genetic/extrinsic occupied lesions) characterized by complete loss of aqueductal CSF signal at any level (obstruction), aqueduct funneling, enlarged inferior third ventricular recesses, enlargement of the lateral

ventricles and third ventricle,^{11,12} in conjunction with increased head circumference and/or cerebral size for gestational age, were incorporated as a control group. The flow chart of the included cases is presented in Fig 1.

Fetal MRI

In vivo fetal MRI was performed according to the ISUOG Practice Guidelines¹³ by using 1.5T or a 3T scanner (Ingenia or Achieva with a 32-channel body coil; Philips Healthcare). In each case, an EPI-T2*-weighted blood-sensitive sequence (TE: 53 ms, TR: 3000 ms, acquisition matrix: 160 × 95 voxels, field of view: 230 mm, NSA: 2, flip angle 90°) was performed in at least 2 perpendicular planes resulting in an in-plane resolution of 0.62–1.0 mm (section thickness 4.0 mm). Routine fetal

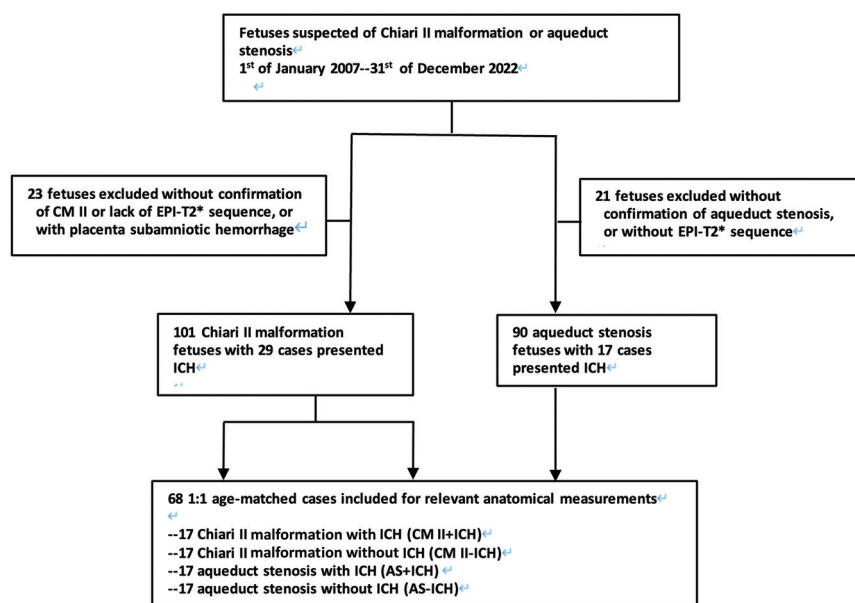


FIG 1. Flow chart of included fetuses with CM II and AS.

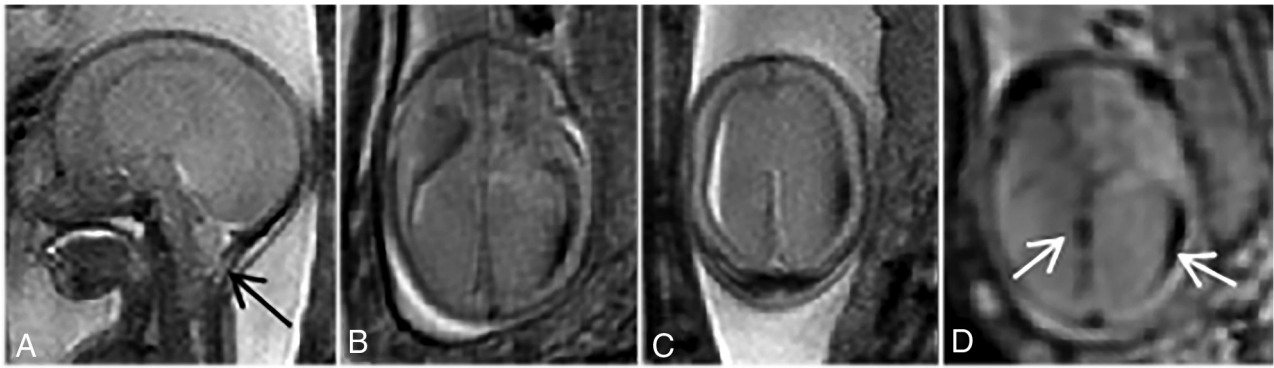


FIG 2. Prenatal MRI of a fetus with CM II and ICH. CM II with ICH case at gestational week 20 + 6. *A*, T2-weighted-FSE image shows the narrowing posterior cranial fossa, accompanied by a protrusion sign of the atlanto-occipital membrane (black arrow). Brain parenchyma hyperintensity indicates edematous changes, with the disappearance of lamination. The outer CSF spaces appear depleted. Intraventricularly observable levels of bloody fluid with varying degrees of sedimentation on both sides, concomitant with markedly dilated lateral ventricles, are illustrated on both T2-SSFSE and EPI-T2* blood-sensitive sequences.

head sequences of T2-weighted single-shot fast spin-echo (SSFSE) and steady-state free precession (SSFP) were also performed (Online Supplemental Data). Specific absorption rate levels did not exceed 2.0 W per kilogram of body weight.

MR Image Analysis

The retrospective classification of intracranial ICH was conducted independently by 2 experienced fetal neuroradiologists (D.P. and H.S., with 35 and 6 years of experience in fetal imaging, respectively), based on the following characteristics: low signal intensity on EPI-T2*-weighted blood-sensitive sequence in at least 2 perpendicular planes (Fig 2) or plus hypointensity (compared with adjacent parenchyma) on T2-TSE sequence. To distinguish hemorrhage from congested veins, a discontinuous signal loss and an asymmetric pattern can serve as differentiating factors (Fig 2, Online Supplemental Data). The presence of hemorrhage, congested veins (in comparison to the control group), and related conditions including subependymal heterotopia, hydrocephalus (in cases of CM II in which hydrocephalus is present, it is noteworthy that side ventricle sizes are often within 10 mm; hydrocephalus in this context is defined as the third ventricle width ≥ 4 mm¹⁴), and brain vasogenic edema were recorded. Venous sinus stenosis was evaluated by using age-matched normal brain fetuses from the existing database¹⁵ as a comparison (Online Supplemental Data). The readers were blinded to the fetal MRI findings and postnatal outcomes. Disagreements were resolved by consensus. Interrater variability analysis was performed.

Vasogenic edema was defined as parenchymal hyperintensity compared with age-matched normal cases on T2-weighted sequences,¹⁶ blurring of lamination, and depleted outer CSF spaces-dry brain (Figs 2 and 3, Online Supplemental Data).

Morphometric Measurements (Inner/Outer CSF Spaces, Posterior Fossa, Venous Structure)

A systematic analysis of CM II and spinal defect characteristics was conducted¹⁷ and compared between CM II with and without ICH cases. We selected 1:1 age-matched (± 5 gestational days) fetuses from CM II with and without ICH cases, as well as AS with and without ICH cases for relevant anatomic measurements,

including outer CSF spaces, maximum atrium width, third ventricle width, maximum diameter of the posterior fossa, and clivus-supraocciput angle,² which was performed by a single radiologist (H.S.) (Online Supplemental Data). These measurements were repeated and averaged for statistical analysis in the respective age-matched groups (CM II+ICH, CM II-ICH, AS+ICH, and AS-ICH). Morphometric measurements were rerated regarding intrarater variability analysis after 2 months. Additionally, cross-sectional areas of both the jugular vein (at the level of the atlantoaxial joint, SSFP sequence)¹⁸ and the superior sagittal sinus (average measurements from 3 slices above the torcular level, T2-SSFSE sequence)¹⁹ were assessed.

Statistics Analysis

Statistical analysis was carried out by using SPSS Statistics for Windows, v. 25 (IBM). Quantitative variables were compared by using the Student *t* test for independent samples, corrected for gestational age; qualitative variables were compared by using Pearson χ^2 .

ANOVA with post hoc Bonferroni testing was used for morphometric measurements, and effect sizes were calculated. Cohen κ assessed interrater agreement. Regression analysis was used to examine the association between dependent variables. Principal component analysis (PCA) was used for multivariate analysis and data visualization. Statistical analysis was performed by a statistical analyst with significant statistical expertise (M.W.).

Co-Occurrence Network of CM II with ICH

To visualize the phenotypic network associated with CM II with ICH and to distinguish it from AS with ICH, we conducted a co-occurrence analysis through Matlab R2021b19 (MathWorks) by using the data of 29 CM II+ICH cases and replicated the process in the 17 AS+ICH cases. The co-occurrence matrix was constructed by extracting co-occurrence patterns from fetal MRI diagnostic features, as documented by co-authors D.P. and G.K., possessing 35 and 16 years of experience in fetal imaging, respectively. Additionally, morphometric measurements mentioned earlier were also incorporated into the matrix. This analysis specifically focused on identifying co-occurrence patterns of “ICH”

Table 1: Fetal demographics and MRI characteristics

Characteristics	Fetuses with CM II (n = 101)	Fetuses with AS (n = 90)	P
Male fetuses (%)	47/101 (46.5)	42/90 (46.7)	.669
Median gestational age at fetal MRI (weeks)	24.4 (16.7–37.3)	22.8 (17.1–41)	.138
Timing of MRI			
≤26 weeks	70	66	
>26 weeks	31	24	
Incidence of ICH			
All gestational ages (%)	29/101 (28.7)	17/90 (18.9)	.023
≤26 weeks (%)	20/71 (28.1)	14/64 (21.8)	.044
>26 weeks (%)	9/30 (30)	3/26 (11.5)	.016

with other comorbidity features within each case. Subsequently, this data set was utilized to create an ICH feature-centric co-occurrence network graph by using Gephi software (<https://gephi.org>). In this network, image features served as nodes, and edges represented their comorbidity, weighted by the frequency of co-occurrence, as derived from the previously imported matrix.

RESULTS

Fetal Characteristics and Outcomes

A total of 101 fetuses with CM II and 90 controls with AS at a median gestational age of 24.4 weeks and 22.8 weeks ($P = .138$) were included (Fig 1, Table 1). Prenatal diagnoses of CM II and AS were confirmed through postnatal or postmortem imaging, or autopsy, and follow-up ranged from 5 days to 16 years. Forty-nine fetuses in the AS group had postnatal correlations, 11 of 49 with hemorrhage in the cerebral aqueduct, 13 of 49 with rhombencephalon synapsis, 8 of 49 with cerebellar dysplasia, 13 of 49 confirmed X-linked aqueduct stenosis (LICAM/MASA syndrome), and 4 of 49 with unknown genesis.

The prevalence of ICH was higher in all gestational ages (summarized in Table 1) compared with AS controls ($P = .023$). The incidence of ICH was slightly but not significantly higher in older (>26 weeks) fetuses ($P = .213$) on comparison between CM II with and without ICH fetuses. Agreement between raters for ICH classification was substantial ($\kappa = 0.92$, $P < .001$).

The 47 of 101 CM II cases (54/101 abortions) received in utero (5/47) or postnatal repair surgery (42/47). In the CM II+ICH group, 17 of 18 cases received CSF shunting, 1 case also underwent expansion of the posterior cranial fossa surgery. Two cases developed epilepsy. Five cases in the CM II+ICH group had a motor functional level worse than anatomically expected.

Forty-seven cases underwent postnatal MRI (Online Supplemental Data). Prenatally suspected heterotopia was confirmed via postnatal MRI (Online Supplemental Data). Fifteen of 47 (32%) exhibited postnatal ICH (12 had prenatal ICH), with 6 of 15 presenting with postnatal brain hemorrhagic infarctions, resulting in subsequent tissue loss. One case in the CM II+ICH group developed transverse sinus thrombosis (Online Supplemental Data). Three cases with transverse sinus stenosis exhibited abnormal drainage patterns of the superior sagittal sinus, and 1 case developed venous malformation. Seven subjects still presented transverse sinus stenosis after shunting (Online Supplemental Data).

Eleven CM II cases underwent post-mortem MRI. Transverse sinus stenosis and congestion in the deep ventricular veins and medullary veins in CM II+ICH cases were identified compared with the CM II-ICH and AS cases in postmortem T2WI and SWI sequences (Online Supplemental Data).

MR Image Analysis

Distinct Features of ICH. The location of most ICH in CM II and AS cases was along the ependyma in dotted/re-

gional patterns, with some affecting the periventricular zone or presenting blood-fluid levels in the ventricles, notably, 8 cases in the CM II group also affected the plexus, accompanied by adjacent congested veins (Fig 3 and Table 2, Online Supplemental Data). ICH was all detected by EPI-T2* blood-sensitive sequences, with 3 cases also showing up on T2-SSFSE or T1WI sequences. Fifteen of 29 (52%) CM II+ICH cases presented dilation (compared with the normal age-matched fetuses) of the subependymal veins (3/13, 23%), plexus veins (5/13, 38%), internal cerebral vein (4/13, 30%), superficial cortical veins (3/13, 23%), mostly affected in fetuses older than 25 gestational weeks, and straight sinus (3/13, 23%) via EPI-T2* sequence, which may indicate congestion present in the subsequent postnatal or post-mortem SWI sequence (Figs 2 and 3 and Online Supplemental Data). On the other hand, 18 of 29 (62%) CM II-ICH cases manifested transverse sinus stenosis (Online Supplemental Data), and 27 of 29 (93%) cases were accompanied by superior sagittal sinus stenosis (Online Supplemental Data).

Systematic Analysis of CM II and Spinal Defect Characteristics.

Using all CM II cases, we found significant differences between fetuses with and without ICH in caudal extend of vermis ectopia (13.7 ± 0.61 versus 7.8 ± 0.46 , $P < .001$), protrusion of atlanto-occipital membrane (93% versus 51%, $P < .001$), the incidence of hydrocephalus (90% versus 60%, $P = .003$), subependymal heterotopia (31% versus 12%, $P = .028$), and white matter edema (86% versus 39%, $P < .001$), as summarized in Table 2. Fetuses with ICH showed a slight but insignificant increase in spinal defect size (28.0 ± 3.6 versus 21.0 ± 1.85 mm², $P = .059$). Otherwise, no other significant differences were detected between the 2 groups.

Repeated Measures ANOVA Using Age-Matched Groups'

Morphometric Measurements. Using age-matched groups, CM II+ICH, CM II-ICH, AS+ICH, and AS-ICH (Table 3), revealed significant differences among all groups in external CSF spaces, clivus-supraocciput angle, maximum atrium width ($P < .001$), and third ventricle width ($P = .005$); the AS groups (with and without ICH) exhibited the largest size of both the atrium and third ventricle width. However, the post hoc test did not show statistically significant differences between AS+ICH and AS-ICH for all measurements. The intrarater agreement of the measurements yielded κ values ranging from 0.88 to 0.94 ($P < .001$). The clivus-supraocciput angle exhibited the most significant effect

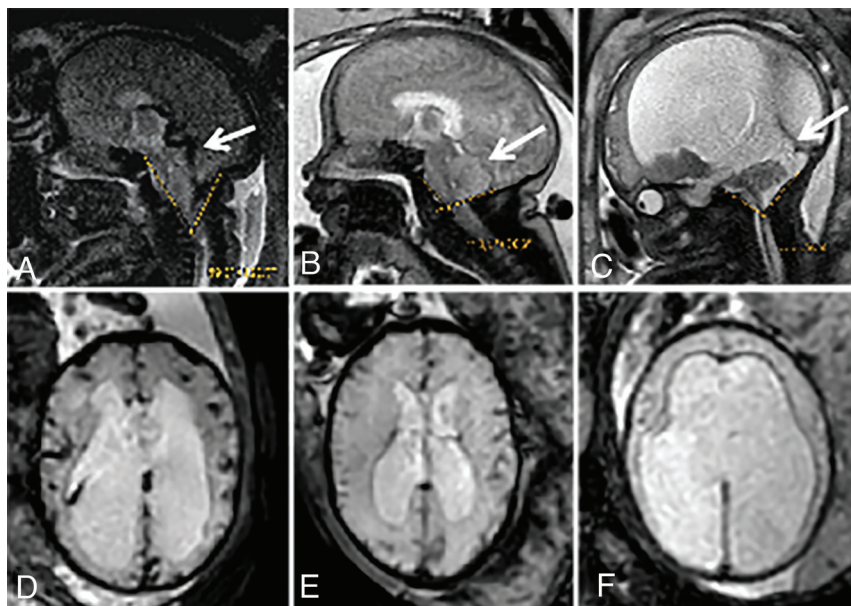


FIG 3. Comparison of clivus-supraocciput angle and venous changes among age-matched fetuses with CM II with and without ICH, and a fetus with AS and ICH. *A and D*, Prenatal MRI scans of a fetus diagnosed with CM II and ICH at gestational age 35 weeks reveal congestion in the straight sinus (arrow) and cortical veins. A sharper clivus-supraocciput angle is depicted in (A). *B and E*, Remarkably, the same imaging modalities in a fetus with CM II without ICH (at gestational age 35 + 3 weeks) show a larger clivus-supraocciput angle without congestion in the straight sinus (arrow) and cortical veins, as seen in the ICH case. *C and F*, Prenatal MRI of a fetus with AS and ICH performed at gestational age 33 weeks depicts normal conditions of the straight sinus (arrow) and cortical veins. Noteworthy are the more rounded posterior horns compared with the distinct pointed posterior horns in the CM II cases.

Table 2: Systematic analysis of CM II and spinal defect characteristics and comparisons between cases with and without ICH

Parameters	CM II with ICH (n = 29)	CM II without ICH (n = 72)	P ^a
Male fetuses (%)	45 (13/29)	48 (35/72)	.730
Median gestational age at fetal MRI (weeks)	25.7 (16.7–35.9)	24.1 (18–37.3)	.338
Incidence of hydrocephalus (%)	90 (26/29)	60 (43/72)	.003
Incidence of brain edema (%)	86 (25/29)	39 (28/72)	<.001
Incidence of heterotopia (%)	31 (9/29)	12 (9/72)	.028
Anatomic level (%)			
Sacral	45 (13/29)	38 (27/72)	.496
Lumbar	31 (9/29)	50 (36/72)	.083
Thoracic	24 (7/29)	12 (9/72)	.251
Size of defect (mm)	28.0 ^b ± 1.95	21.0 ^b ± 1.49	.059
Vermian displacement (%)			
C1–C3	45 (13/29)	56 (40/72)	.329
C4–C7	55 (16/29)	44 (32/72)	.329
Depth of vermis downward displacement (mm)	13.7 ^b ± 0.61	7.8 ^b ± 0.46	<.001
Protrusion sign of atlanto-occipital membrane (%)	93 (27/29)	51 (37/72)	<.001

Note:—Data are given as median (range), n (%) or mean ± standard deviation (SD).

^a Comparison between with and without ICH cases: quantitative variables compared by using Student *t* test for independent samples; qualitative variables compared by using Pearson χ^2 .

^b Estimated means based on an average gestational age = 24.3.

size regarding ICH (Cohen *d* = −2.049, Hedges correction = −1.951). Regression analysis revealed a positive correlation between the cross-sectional areas of the superior sagittal sinus and outer CSF spaces (Online Supplemental Data).

PCA showed 3 separate clusterings of these 4 age-matched groups (Fig 4), the components = 7. Notably, the AS+ICH and AS-ICH groups were not distinguishable.

Co-Occurrence Network of ICH. The co-occurrence networks of MRI diagnostic features in both CM II+ICH and AS+ICH cases were visualized by using Gephi software (Fig 5). While the AS network is mainly centered around aqueduct blockage, in the more complex of CM II network, spinal bony defect, small posterior fossa, and vermis ectopia emerge as core features²⁰ displaying maximum size of nodes. And the connections among them are the thickest indicating their strong co-occurrence. Additionally, there are more contributing involved including reduced outer CSF spaces, the protrusion sign of the atlanto-occipital membrane, venous congestion, and venous sinus stenosis.

DISCUSSION

In this study, in line with the findings of Didier et al,⁶ we identified ICH in 29 of 101 (29%) CM II cases by using the EPI-T2* blood-sensitive sequence, indicating a higher prevalence compared with the AS group (17/90, 19%, *P* = .023). While the AS+ICH group exhibited the most severe degree of hydrocephalus, the higher incidence of ICH in the CM II group suggests additional contributing factors beyond obstructive CSF dynamics and extreme stretching and thinning of the ventricular wall, which can lead to the impairment of the immature ependyma.^{21,22} Hemorrhages predominantly occurred at the ependyma in both groups, notably, 8 cases in the CM II group also affected the plexus, accompanied by adjacent congested veins (Fig 3, Online Supplemental Data). The presence of dilated veins and sinus stenosis (Online Supplemental Data) suggests the potential role of venous congestion in the CM II group in ICH etiology. The incidence of ICH was slightly but not significantly higher in older (>26 weeks) CM II fetuses (*P* = .213), which could be due to the deeper extent of vermis ectopia accompanied by increased ventriculomegaly,⁶ and vanishing outer CSF spaces tend to develop

in later gestation (bias may exist considering a small sample size in older fetuses). Moreover, anatomic measurements highlight the significance of the sharper clivus-supraocciput angle, which exhibited a substantial effect size concerning ICH in CM II. The co-occurrence network visualizes a more intricate interplay of contributing factors in CM II.

Table 3: Morphometric measurements comparisons among CM II and AS groups

Value	CM II+ICH (n = 17)		CM II-ICH (n = 17)		AS+ICH (n = 17)		AS-ICH (n = 17)		P
	Mean	SD	Mean	SD	Mean	SD	Mean	SD	
External CSF spaces	10.7	4.2	16.8	6.8	33.8	6.0	32.9	5.3	<.001
Maximum atrium width (mm)	18.6	5.2	12.4	3.8	23.2	5.2	24.3	5.5	<.001
Third ventricle width (mm)	5.7	2.0	3.9	3.0	6.9	2.8	6.2	2.6	.005
Maximum diameter of the posterior fossa (mm)	22.2	4.5	22.2	4.4	30.4	7.1	30.6	6.9	<.001
Clivus-supraocciput angle (degree)	54.3	8.7	73.2	7.3	90.7	7.9	89.7	8.1	<.001
Cross-section area of jugular vein (mm ²)	6.8	2.2	6.8	2.4	5.9	1.2	6.2	1.2	.322
Cross-section area of superior sagittal sinus (mm ²)	3.9	1.7	5.1	2.7	13.2	6.6	12.4	6.5	<.001

Note:—SD indicates standard deviation, measurement of the cross-section area of the jugular vein was averaged left and right sides.

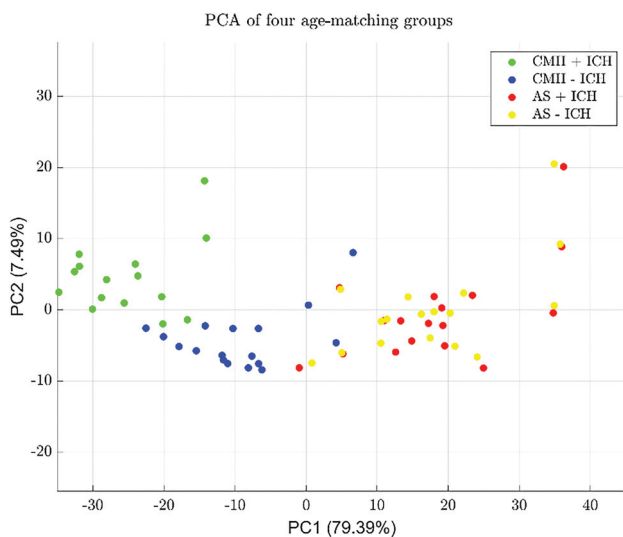


FIG 4. PCA showed 3 separate clusterings of these age-matched groups: group 1: CM II+ICH; group 2: CM II-ICH; group 3: AS+ICH; group 4: AS-ICH; notably AS+ICH and AS-ICH groups cannot be separated. Components = 7.

Deeper extent of vermis ectopia, a significantly higher frequency of hydrocephalus and subependymal heterotopia, as well as brain vasogenic edema, and a more frequent occurrence of the protrusion sign of the atlanto-occipital membrane were found in the CM II+ICH group. The elongation and kinking of the medulla oblongata in CM II, along with increased intraventricular pressure—partly due to associated aqueductal stenosis—may result in brainstem compression and partial obstruction of venous return, leading to tissue edema. The proliferation of the capillary network in developing brain tissue can also be impaired, leading to both ischemic and hemorrhagic microinfarcts (Online Supplemental Data). Damaged ependyma may fail to regulate the transport of fluid, ions, and small molecules between cerebral parenchyma and ventricular fluid, contributing to the higher incidence of hydrocephalus in the ICH group.^{23,24} The posterior and downward protrusion of the vermis creates a concavity in the atlanto-occipital membrane, resembling a notch just below the level of the torcula (Online Supplemental Data), where the transverse sinus is situated. This explains the occurrence of transverse sinus stenosis in certain cases (Online Supplemental Data).

On the other hand, the cross-sectional areas of the jugular vein did not exhibit significant variation among the groups, suggesting that venous drainage blockage likely occurs at the cranial cervical

junction. These findings (evidence of blockage affecting inner and outer CSF outflow as well as venous drainage) collectively indicate the potential existence of a complex feedback loop in CM II cases.⁵ As illustrated by the “co-occurrence network,” this cycle is characterized by a hypoplastic posterior cranial fossa and cerebellar prolapse that generates abnormal tension within the constrained bone container. Consequently, this tension leads to the compression of crucial structures such as the transverse sinus and superior sagittal sinus, which are attached to the crista galli at the interhemispheric space just beneath the cranial vault^{8,25} with the side walls lacking muscle structure that could be compressed by the expanding and swollen parenchyma, resulting in vasogenic edema. Simultaneously, anatomic venous sinus obstruction can further elevate venous outflow resistance,^{26,27} resulting in increased venous pressure that may contribute to hemorrhage and the development of communicant-type hydrocephalus. This is compounded by defective CSF absorption due to increased venous pressure, with the elevated venous pressure itself primarily resulting from the constriction of the posterior cranial fossa structures.³ Although vermis ectopia is not a true herniation because intracranial hypertension is not the primary mechanical force causing this displacement,¹ venous congestion and subsequent edema may exacerbate the vermis ectopia (Online Supplemental Data).

Both mechanisms are known to hinder venous drainage leading to deep venous congestion and dilation,^{3,28} where mostly the deep paraventricular veins could be affected, because fetal microcirculation may lack full development of the cortical venous drainage.²⁹ More clinical morbidity and postnatal disability happened in the CM II with ICH cases, which could be attributed to more severe morphologic deformation: a deeper extent of vermis ectopia and a sharper clivus-supraocciput angle, leading to more severe CSF and venous drainage blockage in the posterior fossa. In some cases, hemorrhagic infarction was suspected to occur after shunt placement, underscoring the importance of including MRV in the prenatal diagnosis of CM II with ICH to evaluate venous conditions before shunting. Surgeons may need to exercise caution when adjusting the speed and pressure during CSF shunting to mitigate blood pressure fluctuations and should closely monitor the child postoperatively. Addressing this complex interplay further supports the concept of prenatal surgery, which leads to an expansion of outer CSF spaces and presumably the reestablishment of proper CSF dynamics^{30,31} and improves the venous drainage system (Online Supplemental Data). The

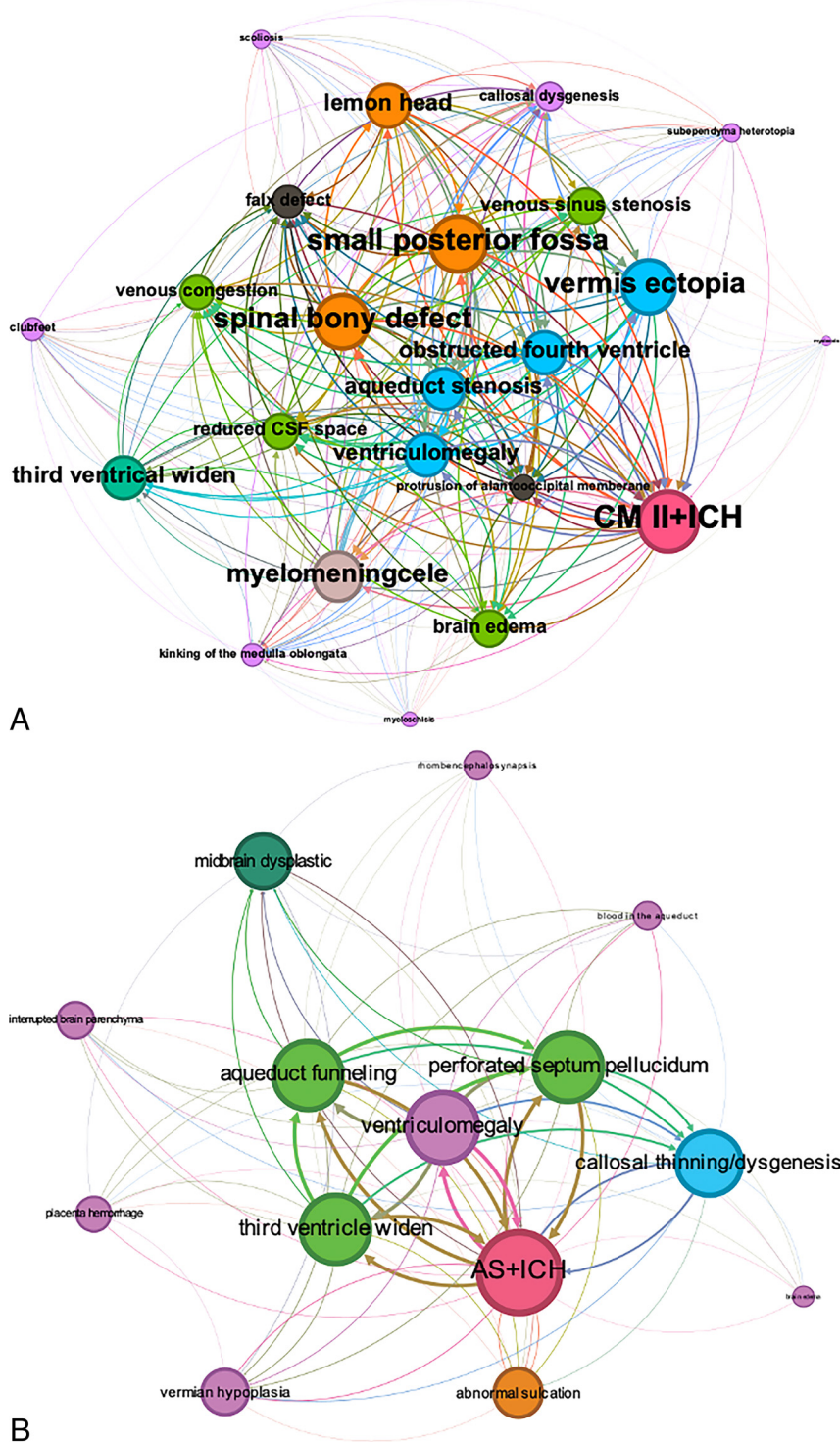


FIG 5. Comparison of co-occurrence network among fetal MRI features of CM II with ICH, and AS with ICH. The CM II network displays a higher level of complexity, involving interactions between spinal, skull, and brain anatomic structures, while the AS network is primarily influenced by CSF blockage. We used “Betweenness Centrality” to determine node colors, where larger nodes indicate more connections, representing a higher degree of co-occurrence with other features. The weight of each edge corresponds visually to the thickness of the connecting lines and represents the pair-wise frequency of co-occurrence.

study's findings hold promise for clinical practice, potentially optimizing the selection of surgical intrauterine repair. In some institutions, ICH has been considered unrelated to the primary

intracranial hemorrhage in CM II, as well as the radiographers of the Division of Neuro- and Musculoskeletal Radiology at the Medical University of Vienna for their enthusiastic support.

disease and excluded from surgery.¹⁰ The study's insights into ICH prevalence and its association with CM II challenge this notion.

Our study has several limitations. First, incorporating AS as a control might be controversial regarding the parenchymal, meningeal, and osseous architecture differences although it aligns with the aim of this study, namely, to validate the common prevalence of ICH and contributing factors in CM II comparing another cohort presenting ICH and hydrocephalus. Second, although not significantly different, the younger gestational age of the AS fetuses might potentially influence the observed prevalence of ICH in this study. Third, different field strengths led to different parameters for the GRE sequence, the potential for interval hemorrhage, and unavoidable differences in the timing of imaging could have influenced the prevalence of ICH between groups. Fourth, our comparably large cohorts of CM II and AS were collected over a relatively long time span without having undergone in utero repair. This is advantageous, as this cohort may serve as “historical” controls with high imaging quality, however disadvantageous as it does not allow for any conclusion on the impact of fetal surgery on the course of intraventricular hemorrhage in CM II. We are convinced that the examined phenomenon and imaging features allow for interesting comparative and outcome studies in cohorts treated surgically.

CONCLUSIONS

ICH is intricately linked to CM II in the fetal stage, with a complex interplay of factors contributing to a vicious cycle of venous congestion and altered CSF dynamics. Pathophysiologic alterations of ICH underlie a more severe phenotype of CM II, which should be considered a candidate for in utero surgery.

ACKNOWLEDGMENTS

The authors would like to thank Professor Harvey. B. Sarnat for the comment on the potential etiology of

REFERENCES

- Sarnat HB. Disorders of segmentation of the neural tube: Chiari malformations. *Handb Clin Neurol* 2008;87:89–103 [CrossRef Medline](#)
- Woitek R, Dvorak A, Weber M, et al. MR-based morphometry of the posterior fossa in fetuses with neural tube defects of the spine. *PLoS One* 2014;9:e112585 [CrossRef Medline](#)
- Tamburrini G, Frassanito P, Iakovaki K, et al. Myelomeningocele: the management of the associated hydrocephalus. *Childs Nerv Syst* 2013;29:1569–79 [CrossRef Medline](#)
- McLone DG, Dias MS. The Chiari II malformation: cause and impact. *Childs Nerv Syst* 2003;19:540–50 [CrossRef Medline](#)
- Fukuoka T, Nishimura Y, Hara M, et al. Chiari Type 1 malformation-induced intracranial hypertension with diffuse brain edema treated with foramen magnum decompression: a case report. *NMC Case Rep J* 2017;4:115–20 [CrossRef Medline](#)
- Didier RA, Martin-Saavedra JS, Oliver ER, et al. Fetal intraventricular hemorrhage in open neural tube defects: prenatal imaging evaluation and perinatal outcomes. *AJNR Am J Neuroradiol* 2020;41:1923–29 [CrossRef](#)
- Zamlynski J, Olejek A, Koszutski T, et al. Comparison of prenatal and postnatal treatments of spina bifida in Poland—a non-randomized, single-center study. *J Matern Fetal Neonatal Med* 2014;27:1409–17 [CrossRef](#)
- Cinalli G, Russo C, Vitulli F, et al. Changes in venous drainage after posterior cranial vault distraction and foramen magnum decompression in syndromic craniosynostosis. *J Neurosurg Pediatr* 2022;30:330–41 [CrossRef Medline](#)
- Lauzier DC, Chiang SN, Chatterjee AR, et al. Idiopathic intracranial hypertension and vascular anomalies in Chiari I malformation. *Neurosurg Clin N Am* 2023;34:175–83 [CrossRef](#)
- Putbrese B, Kennedy A. Findings and differential diagnosis of fetal intracranial haemorrhage and fetal ischaemic brain injury: what is the role of fetal MRI? *Br J Radiology* 2017;90:20160253 [CrossRef Medline](#)
- Heaphy-Henault KJ, Guimaraes CV, Mehollin-Ray AR, et al. Congenital aqueductal stenosis: findings at fetal MRI that accurately predict a postnatal diagnosis. *AJNR Am J Neuroradiol* 2018;39:942–48 [CrossRef Medline](#)
- Barkovich AJ, Newton TH. MR of aqueductal stenosis: evidence of a broad spectrum of tectal distortion. *AJNR Am J Neuroradiol* 1989;10:471–76
- Prayer D, Malinger G, De Cotte L, et al. ISUOG Practice Guidelines (updated): performance of fetal magnetic resonance imaging. *Ultrasound Obstet Gynecol* 2023;61:278–87 [CrossRef](#)
- Garel C. *MRI of the Fetal Brain: Normal Development and Cerebral Pathologies*. Stuttgart, Germany: Springer-Verlag; 2004.
- Stuempflen M, Taymourtash A, Kienast P, et al. Ganglionic eminence: volumetric assessment of transient brain structure utilizing fetal magnetic resonance imaging. *Ultrasound Obstet Gynecol* 2023;62:405–13 [CrossRef Medline](#)
- Shi H, Prayer F, Kienast P, et al. Multiparametric prenatal imaging characterization of fetal brain edema in Chiari II malformation might help to select candidates for fetal surgery. *Eur Radiology* Published online April 24, 2024. [CrossRef](#)
- Avesani G, Perazzolo A, Elia L, et al. Fetal MRI prior to intrauterine surgery of open neural tube defects: what does the radiologist need to know. *Radiology Med* 2022;128:113–24 [CrossRef Medline](#)
- Fu SJ, Xu JB, Liu X, et al. Quantitative evaluation of a cross-sectional area of the fetal straight sinus by magnetic resonance imaging and its clinical value. *Front Neurol* 2022;13:875402 [CrossRef Medline](#)
- Bateman GA, Lechner-Scott J, Bateman AR. Modelling of the dilated sagittal sinuses found in multiple sclerosis suggests increased wall stiffness may be a contributing factor. *Sci Rep* 2022;12:17575 [CrossRef Medline](#)
- Barabasi AL, Gulbahce N, Loscalzo J. Network medicine: a network-based approach to human disease. *Nat Rev Genet* 2011;12:56–68 [CrossRef Medline](#)
- Sarnat HB. Regional differentiation of the human fetal ependyma: immunocytochemical markers. *J Neuropathol Exp Neurol* 1992;51:58–75 [CrossRef Medline](#)
- Sarnat HB. Histochemistry and immunocytochemistry of the developing ependyma and choroid plexus. *Microsc Res Tech* 1998;41:14–28 [CrossRef](#)
- Sarnat HB. Ependymal reactions to injury. A review. *J Neuropathol Exp Neurol* 1995;54:1–15 [CrossRef Medline](#)
- Del Bigio MR. Ependymal cells: biology and pathology. *Acta Neuropathol* 2010;119:55–73 [CrossRef Medline](#)
- Lublinsky S, Friedman A, Kesler A, et al. Automated cross-sectional measurement method of intracranial dural venous sinuses. *AJNR Am J Neuroradiol* 2016;37:468–74 [CrossRef Medline](#)
- Markey KA, Mollan SP, Jensen RH, et al. Understanding idiopathic intracranial hypertension: mechanisms, management, and future directions. *Lancet Neurol* 2016;15:78–91 [CrossRef](#)
- Zhao K, Gu W, Liu C, et al. Advances in the understanding of the complex role of venous sinus stenosis in idiopathic intracranial hypertension. *J Magn Reson Imaging* 2022;56:645–54 [CrossRef](#)
- Conner ES, Foley L, Black PM. Experimental normal-pressure hydrocephalus is accompanied by increased transmantle pressure. *J Neurosurg* 1984;61:322–27 [CrossRef Medline](#)
- Okudera T, Huang YP, Fukusumi A, et al. Micro-angiographical studies of the medullary venous system of the cerebral hemisphere. *Neuropathology* 1999;19:93–111 [CrossRef Medline](#)
- Mufti N, Aertsen M, Ebner M, et al. Cortical spectral matching and shape and volume analysis of the fetal brain pre- and post-fetal surgery for spina bifida: a retrospective study. *Neuroradiology* 2021;63:1721–34 [CrossRef Medline](#)
- Jakab A, Payette K, Mazzone L, et al. Emerging magnetic resonance imaging techniques in open spina bifida in utero. *Eur Radiology Exp* 2021;5:23 [CrossRef Medline](#)